ISSN 0035-4511, Volume 49, Number 3

Rheol Acta (2010) 49:245–254
DOI 10.1007/s00397-009-0409-1

ORIGINAL CONTRIBUTION

Spreading and fingering in a yield-stress fluid during spin coating

Kristi E. Holloway · Hervé Tabuteau · John R. de Bruyn

Received: 22 September 2009 / Accepted: 16 November 2009 / Published online: 9 December 2009

Abstract We study the deformation, spreading, and fingering of small droplets of a yield-stress fluid subjected to a centrifugal force on a rotating substrate. At low rotation rates and for small enough droplets, the droplets deform elastically but retain their essentially circular contact line. For large enough droplet volumes and rotation speeds, however, one or more fingers eventually form and grow at the edge of the drop. This fingering is qualitatively different from the contact line instability observed in other fluids, and appears to be a localized phenomenon that occurs when the stress at some point on the perimeter of the drop exceeds the yield stress.

Keywords Yield stress · Yielding · Instability · Spin coating

Introduction

The process of spin coating involves depositing a volume of fluid on a substrate which is then rapidly rotated, forcing the fluid to spread due to the centrifugal force. Industrially, spin coating is used as a method of forming thin uniform films or coatings. In such applications, it is the late stage of the process, after the liquid–solid–air contact line has spread over the substrate, which is most relevant. The spreading of the contact line during the early stages of spin coating is itself an interesting process, however. As in other flows in which a contact line is driven by an external force, an instability can occur at the contact line of the fluid leading to the formation and growth of fingers. In the case of spin coating (Emslie et al. 1957; Melo et al. 1989; Fraysse and Homsy 1994), this can lead to uneven coating thicknesses. Fingering instabilities also occur during flow down an inclined plane (Troian et al. 1989a; Schwartz 1989; de Bruyn 1992; Jerrett and de Bruyn 1992; de Bruyn et al. 2002) and spreading due to Marangoni forces (Troian et al. 1989b). Although fingering in Newtonian fluids has been studied extensively (Emslie et al. 1957; Melo et al. 1989; Troian et al. 1989a; Schwartz 1989; de Bruyn 1992; Jerrett and de Bruyn 1992; Fraysse and Homsy 1994; Spaid and Homsy 1996, 1997; McKinley et al. 1999; Togashi et al. 2001; Wang and Chou 2001; McKinley and Wilson 2002; Holloway et al. 2007), there have been rather few investigations of fingering in non-Newtonian fluids in general (Acrivos et al. 1960; Lemaire et al. 1991; Fraysse and Homsy 1994; Borkar et al. 1994; Spaid and Homsy 1994, 1996, 1997) and yield-stress fluids in particular (Jenekhe and Schuldt 1985; Burgess and Wilson 1996; Tsamopoulos et al. 1996; Lindner et al. 2000; de Bruyn et al. 2002; Tabuteau et al. 2007a; Balmforth et al. 2007). In this paper, we study the spreading and fingering of small droplets of Carbopol, a yield-stress polymer gel, subjected to a centrifugal force. While pervious work

K. E. Holloway · J. R. de Bruyn
Department of Physics and Physical Oceanography, Memorial University of Newfoundland, St. John's, Newfoundland and Labrador, Canada A1B 3X7

H. Tabuteau · J. R. de Bruyn (✉)
Department of Physics and Astronomy, The University of Western Ontario, London, Ontario, Canada N6A 3K7
e-mail: debruyn@uwo.ca

H. Tabuteau
Laboratoire de Colloïdes, Verres, et Nanomatériaux, UMR 5587, Montpellier, France

(de Bruyn et al. 2002; Tabuteau et al. 2007a; Balmforth et al. 2007) has involved situations in which the driving force was much larger than the force due to the yield stress, our intent is to study the stability of the contact line in the regime in which the two forces are comparable in magnitude.

While Newtonian fluids are characterized by a constant viscosity η, non-Newtonian fluids display both viscous and elastic behavior, and in general have a viscosity that depends on the strain rate $\dot{\gamma}$. Acrivos et al. (1960) studied the evolution of fluid profiles for power-law fluids undergoing spin coating. Homsy and coworkers (Fraysse and Homsy 1994; Spaid and Homsy 1994, 1996, 1997) studied the spreading and fingering of an elastic fluid drop during spin coating both experimentally and theoretically. Borkar et al. (1994) studied the spin coating of viscoelastic fluids experimentally and theoretically, but make no mention of a fingering instability.

Yield-stress fluids flow when the shear stress τ exceeds a threshold value referred to as the yield stress τ_0 (or equivalently when the shear strain γ exceeds the yield strain γ_0); below this value, the fluid responds elastically to the applied stress, that is, it acts like a soft solid. Numerical studies of spin coating in yield-stress fluids have shown that the height of an initially uniform film becomes nonuniform during the spinning process (Jenekhe and Schuldt 1985; Burgess and Wilson 1996; Tsamopoulos et al. 1996). Experiments performed with a yield-stress fluid agreed with these predictions (Jenekhe and Schuldt 1985). Tabuteau et al. (2007a) studied the spreading of yield-stress fluids both theoretically and experimentally. They calculated a critical angular velocity ω_c for the yielding of the material under different geometrical conditions. Experimentally, they studied the effect of substrate roughness, angular acceleration, yield stress, and sample size on the spreading. While their work focussed mainly on spreading, they also observed the formation of fingers around the perimeter of the sample at high enough angular velocity ω. de Bruyn et al. (2002) studied the fingering instability at the contact line of a yield-stress clay suspension flowing down an inclined plane and compared the experimentally observed wavelength of the instability with the predictions of a model that took into account the yield-stress behavior of the material, and recently Balmforth et al. (2007) have performed a detailed theoretical study of this system.

The details of our experimental apparatus, sample preparation, and sample characterization are presented in the section "Experimental method and materials." Our results are presented in the section "Results" and discussed in the section "Discussion."

Experimental method and materials

The experimental apparatus is identical to that used in our previous experiments on spin coating in a Newtonian fluid (Holloway et al. 2007). The substrate is a transparent, circular sapphire plate 10 cm in diameter. The plate is mounted on a bearing and can be rotated by a computer-controlled microstepper motor. In the work described here, its angular velocity ω is varied in the range 10.5–63 rad/s. The acceleration of the plate is fixed at 168 rad/s^2. The plate reaches its final velocity in 0.0625 s for the lowest speed used and 0.375 s for the highest speed used. Observations indicate that this acceleration time is much less than the time at which fingering begins. Prior to the start of a run, the plate is cleaned with warm, soapy water and rinsed in acetone. A length of fine tubing attached to a syringe pump is mounted in a vertical holder which, using two micrometer-driven translation stages, had previously been precisely positioned above the center of the plate using a dummy substrate with a small hole machined in its center. The syringe pump deposits a specified volume V of fluid onto the substrate at a rate of 1 ml/min. In this work, we studied drop volumes in the range 0.2–1 ml. The existence of a yield stress makes it more difficult to center the drops than was the case with Newtonian fluids (Holloway et al. 2007), but the centering was always accurate to within 5% of the drop radius. The fluid drop is allowed to relax for 5 min before rotation begins.

A shadowgraph optical system is used to visualize the flow. A collimated beam of light from a bright red LED was passed through the sample from below and focused onto a video camera mounted above the substrate. As the images shown below in Figs. 3 and 4 illustrate, this method provides very clear visualization of the perimeter of the fluid drops. The contrast within the fluid drop in these images is due to variations in the slope of the fluid surface (discussed below), which cause the light beam to be deflected. The resolution of the optical system was typically 0.016 cm/pixel.

The fluids studied were aqueous solutions of Carbopol ETD 2050 (Noveon 2002), with concentrations $c = 0.2\%$ and 0.4% by weight. Carbopol is a commercial product used as a thickener, and is based on cross-linked linear polyacrylic acid chains. Carbopol dispersions are highly transparent, facilitating optical flow visualization. They behave as yield-stress fluids due to interactions among a network of micron-sized microgel particles (Carnali and Naser 1992). The samples were prepared by slowly adding Carbopol powder to continuously stirred deionized water. Sodium hydroxide solution was then added to raise the pH to 6.

The solutions were further mixed for several hours with a motorized mixer to completely homogenize the material. At the concentrations used here, the solutions were very weak gels with density equal to $1{,}000 \pm 5$ kg/m^3 at 22°C.

Rheometric characterization of the Carbopol samples was performed using an ARES RHS controlled-strain rheometer equipped with stainless steel concentric cylinders with inner and outer radii of 16 and 17 mm, respectively, and an immersed length of 34 mm. The sample temperature was maintained at 22°C by a temperature-controlled circulating fluid bath. The flow curve was measured by imposing a steady shear and recording the corresponding steady-state stress, starting at high shear rate and working downwards. The linear elastic and viscous moduli, G' and G'', respectively, were measured as a function of frequency by applying a small-amplitude oscillatory shear.

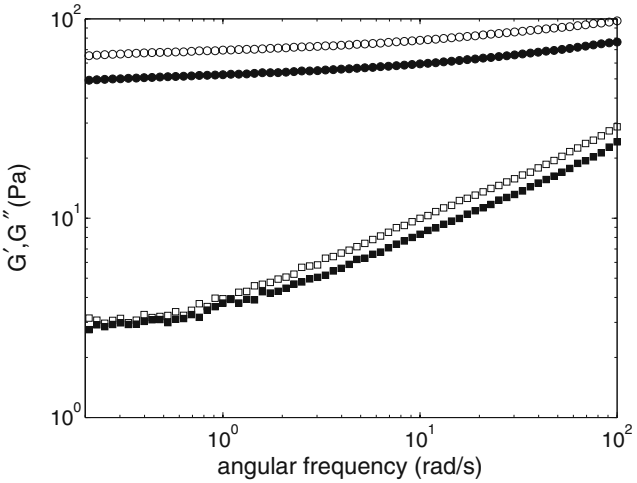

Fig. 2 The elastic modulus G' (*circles*) and viscous modulus G'' (*squares*) as a function of frequency for 0.2% Carbopol (*solid symbols*) and 0.4% Carbopol (*open symbols*)

Results

Rheology

The rheometric measurements show that our Carbopol samples behave as yield-stress fluids with a small but easily measurable yield stress. Figure 1 shows the flow curves (shear stress as a function of strain rate $\dot{\gamma}$) for the two concentrations of Carbopol. In both cases, the data were well described by fits to a Herschel–Bulkley model,

$$\tau = \tau_0 + K\dot{\gamma}^n, \tag{1}$$

where τ_0 is the yield stress, K is the consistency, and n is a power law index. For $c = 0.2\%$, we find $\tau_0 = 1.49 \pm 0.02$ Pa, $K = 5.56 \pm 0.03$ Pa s^n, and $n = 0.434 \pm 0.002$, while for $c = 0.4\%$, we find $\tau_0 = 1.74 \pm 0.16$ Pa, $K = 9.22 \pm 0.33$ Pa s^n and $n = 0.42 \pm 0.02$. For $\tau > \tau_0$, the samples are shear thinning, that is, the viscosity $\tau/\dot{\gamma}$ decreases with increasing strain rate. Figure 2 shows G' and G'' for the two concentrations. In both cases, the elastic modulus is an order of magnitude larger than the viscous modulus and is nearly independent of frequency, as expected for a yield-stress gel.

As noted below, there is evidence to suggest that the rheological properties of the Carbopol change over the course of a spin-coating experiment, likely due to evaporation from the surface of the small drops used in our experiments. This effect is difficult to quantify, particularly since the volume of the droplets is somewhat smaller than that required for rheological characterization, and their surface-to-volume ratio is significantly larger. The rheological data presented here are thus intended only to provide a characterization of our material at the beginning of the experiments.

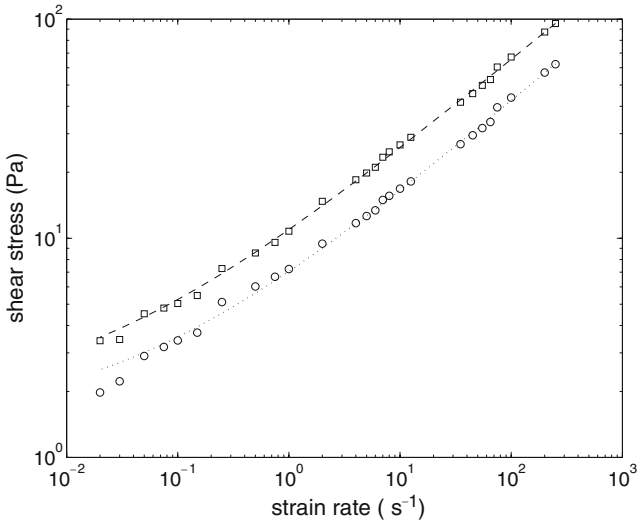

Fig. 1 Mean measured flow curves for $c = 0.2\%$ (*circles*) and $c = 0.4\%$ (*squares*). The *lines* are fits to the data using the Herschel–Bulkley model, Eq. 1

Spreading and fingering

Figure 3 shows a sequence of images from a run using Carbopol with $c = 0.4\%$, $\omega = 47.3$ rad/s, and $V = 0.5$ ml. The edge of the drop is initially close to circular, as shown in Fig. 3a. Since the Carbopol has a

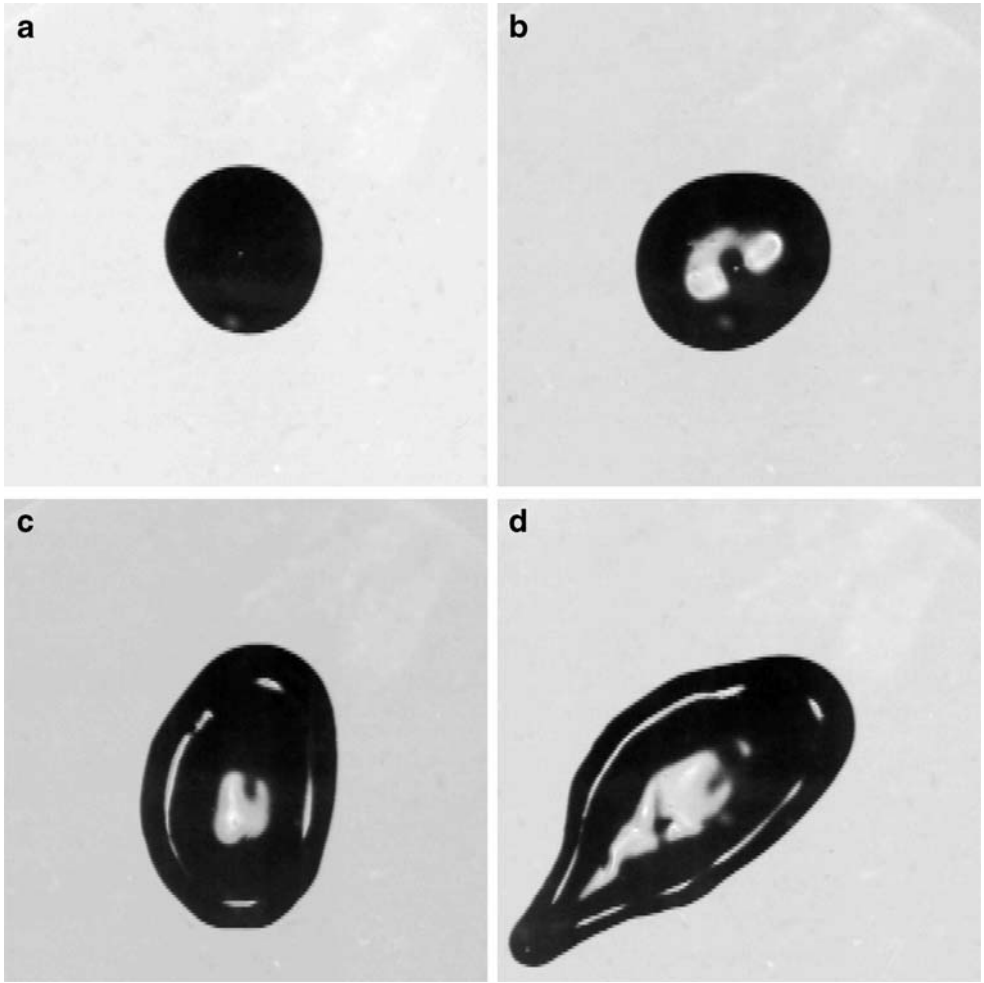

Fig. 3 Images from a run with $c = 0.4\%$ showing the development of a finger as a function of time. For this run, $V = 0.5$ ml and $\omega = 47.3$ rad/s. Images were recorded at **a** 0.17 s, **b** 22.1 s, **c** 59.76 s, and **d** 77.34 s. The Carbopol drop appears dark, with light areas within the drop indicating local maxima or minima in the thickness of the drop. A ridge of fluid, indicated by a light partial ring, can be seen close to the perimeter in **c** and **d**. The field of view is approximately 5.3 cm

yield stress, there were inevitably small deviations from circularity in the initial shape of the drop. These were typically at the level of 5–8% of the drop's radius. When the substrate is spun, the drop spreads uniformly by a small amount under the action of the centrifugal force. For high enough values of V and ω, a single finger eventually forms and grows at the perimeter, as shown in Fig. 3b–d. This is occasionally followed by the later formation of one or more additional fingers. In cases for which fingering occurred, a well-defined roll or ridge was observed to form around the perimeter of the drop, as previously observed for both Newtonian fluids (Melo et al. 1989; Fraysse and Homsy 1994; Holloway et al. 2007) and yield-stress fluids (Tabuteau et al. 2007a). This ridge appears in Figs. 3 and 4 as a bright region close to the perimeter. The shadowgraph images from most runs in which fingering did not occur show a weak flattening of the drops but no clear ridge, while runs in which the drop did not spread at all showed no detectable change in the drop's profile. In the run shown in Fig. 3, and indeed in the majority of runs, only one finger formed over the duration of the experiment. This finger often formed at the location of an initial outward deviation from circularity, but sometimes such deviations initially decreased in size as the drop spread, and the finger eventually appeared elsewhere. In a few cases, one of which is illustrated in Fig. 4, more than one finger appeared. In such cases, the fingers did not form simultaneously, nor were they equally spaced around the perimeter, and there were no systematic trends relating the appearance of multiple fingers to the experimental conditions. Rather, the second and any subsequent fingers appeared to form quite independently of the original finger.

For each of the hundreds of experimental images from a given run, an edge detection algorithm is used to identify the perimeter of the Carbopol drop. The drops are initially very close to circular, and a least-squares routine is used to fit a circle to the perimeter. The center of the fitted circle is allowed to vary depending on the shape of the drop. The radial strain of the drop, given by $\gamma_r = (r_f - r_{f0})/r_{f0}$, where r_f is the radius of

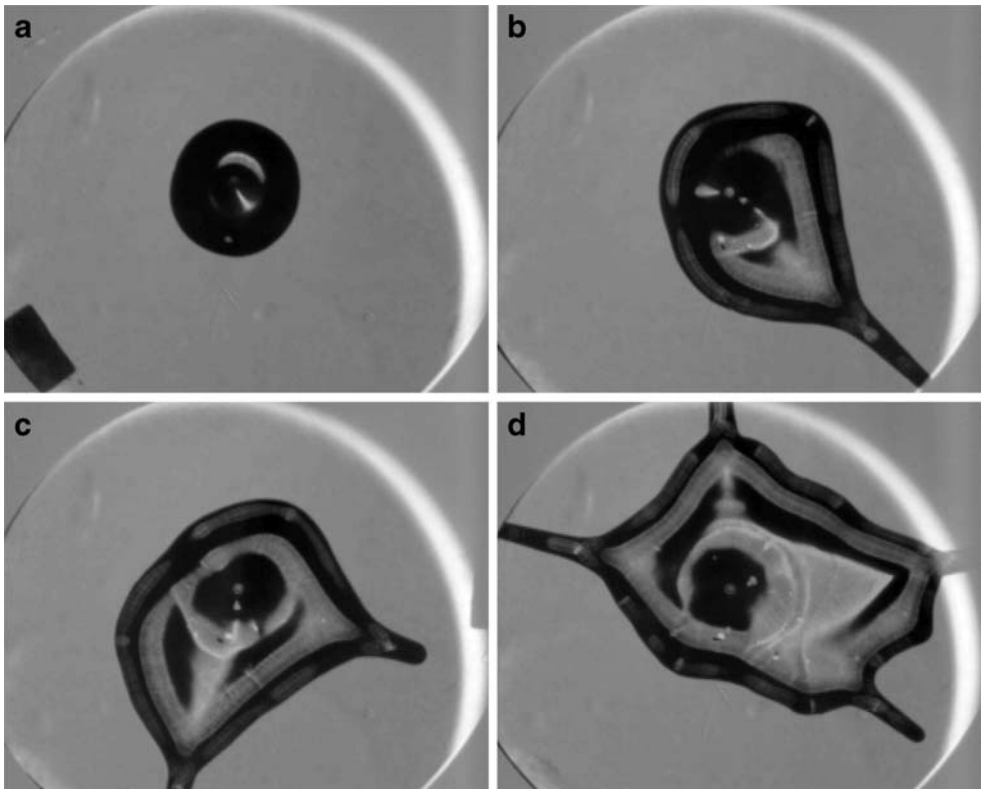

Fig. 4 Images from a run with $c = 0.4\%$ showing the formation and growth of several fingers. Here, $V = 1$ ml and $\omega = 63$ rad/s. Images were recorded at **a** 0.57 s, **b** 2.90 s, **c** 4.57 s, and **d** 11.23 s. The field of view is 8.2 cm

the fitted circle and r_{f0} is its value at the start of the run, is used as a measure of the spreading of the drop. Figure 5 shows γ_r plotted as a function of time for one particular run in which the drop did *not* finger. γ_r initially increases, then reaches a limiting value $\gamma_{r,1}$, which, for the run shown in Fig. 5, is equal to 0.027. The scatter in the data at long times indicates the uncertainty in determining r_f and corresponds to roughly 0.1 pixels. The data are, in general, well described by a simple exponential approach to a limiting value, with a time constant on the order of 100 s. Our measurements show no unambiguous trend in the limiting value of γ_r as a function of ω within our experimental scatter, but the maximum observed value of $\gamma_{r,1}$, for each concentration can be taken as a lower limit on the yield strain in each case. For $c = 0.2\%$, the maximum value of $\gamma_{r,1}$ is 0.066, while for $c = 0.4\%$, it is 0.17.

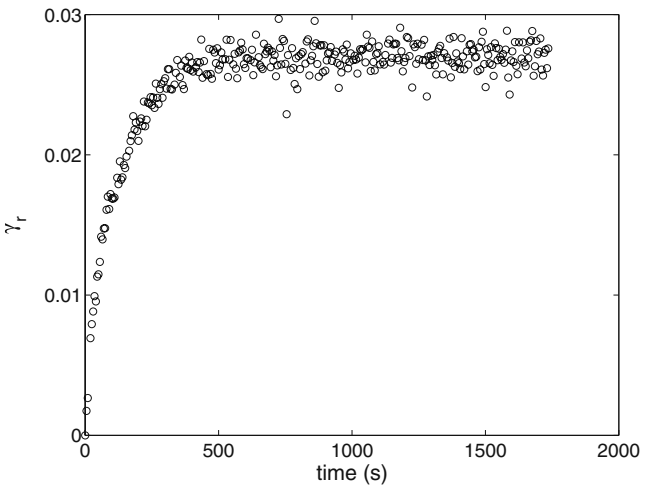

Fig. 5 The radial strain γ_r plotted as a function of time for a drop that did not finger. Here, $c = 0.4\%$, $V = 0.5$ ml, $\omega = 21$ rad/s, and Bn = 5.2

The spreading behavior of drops that do finger is qualitatively different from that shown in Fig. 5. Figure 6a and b show γ_r for $c = 0.4\%$ and several values of ω and V for which fingering was observed. For these runs, the radial strain increases much more rapidly than in the non-fingering case: γ_r exceeds the yield strain (that is, the maximum value of $\gamma_{r,1}$ observed for drops that do not finger) in only a few seconds. The increase is initially linear, and while the slope may decrease as the run progresses, there is no sign of saturation over the duration of the experiment. In general, γ_r increases more rapidly as either ω or V increases.

When fingers start to form, the drops begin to deviate significantly from circularity. From the image analysis described above, we can also determine $r_{\max}$, the maximum distance from the center of the fitted circle to the drop edge, and $\delta_{\max} = (r_{\max} - r_f)/r_f$. $\delta_{\max}$ is the

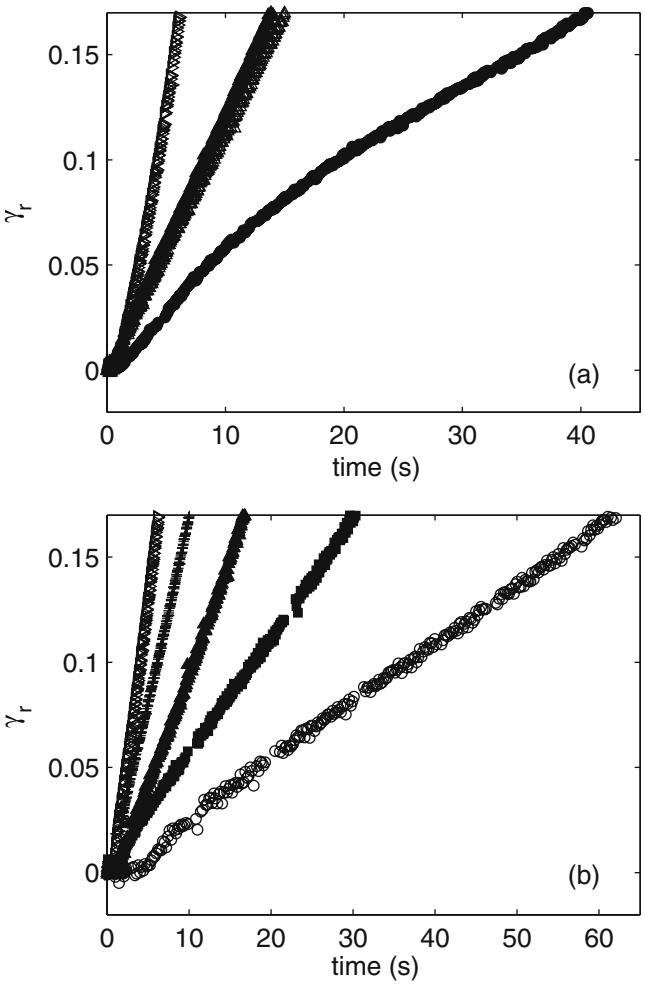

Fig. 6 **a** The radial strain γ_r as a function of time for $c = 0.4\%$ and $V = 0.5$ ml. The *different symbols* represent runs with different ω. From *top* to *bottom*, ω =63, 52.5, 57.8, and 42 rad/s. **b** γ_r as a function of time for $c = 0.4\%$ and $\omega = 52.5$ rad/s. The different symbols represent runs with different V. From *top* to *bottom*, $V = 0.75$, 0.6, 0.4, 0.3, and 0.2 ml

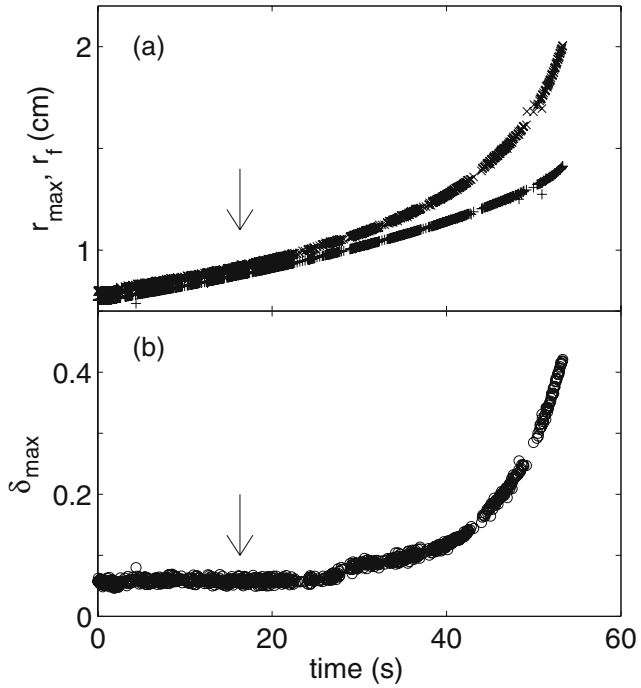

Fig. 7 **a** r_f (+), the best-fit radius of the Carbopol drop, and $r_{\max}$ (×), the maximum radial coordinate of the drop, plotted as a function of time for a run with $c = 0.4\%$, $V = 0.4$ ml, $\omega = 52.5$ rad/s, and Bn = 0.82. **b** $\delta_{\max}$, the maximum deviation from circularity, plotted as a function of time. In both cases the time at which the radial strain reaches 0.17 is indicated by the *arrow*

maximum deviation from circularity and is a measure of the length of the largest finger that forms. Figure 7a is a plot of $r_{\max}$ and r_f as a function of time for one run, while $\delta_{\max}$ is plotted in Fig. 7b. For about the first 20 s of this particular run, both $r_{\max}$ and r_f increase at the same rate while $\delta_{\max}$ remains essentially constant; that is, the drop spreads, but there is no sign of finger growth. After about 25 s, $r_{\max}$ starts to increase faster than the best-fit radius and $\delta_{\max}$ starts to grow, as seen in Fig. 7b. The arrow in Fig. 7 indicates the time at which the radial strain reaches 0.17, the estimated yield strain for this concentration, and in this case, the finger starts to develop shortly after the strain exceeds this value. In some other runs, however, there were signs of a developing finger slightly before the strain reached this value.

Figure 8 is a semi-logarithmic plot of the finger length $\delta_{\max}$ (offset by its small initial value δ_0 at time $t = 0$) plotted as a function of time for a particular run. A fit to a growing exponential of the form $\delta_{\max} - \delta_0 = ae^{\beta t}$ is shown as a dashed line in Fig. 8. Here, the coefficient a and the growth rate β are treated as fitting

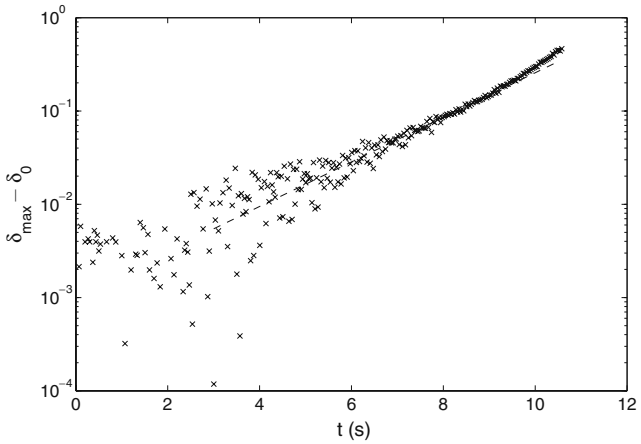

Fig. 8 The length $\delta_{\max}$ of a finger growing in an experiment with $c = 0.4\%$, $V = 0.5$ ml, $\omega = 63$ rad/s, and Bn = 0.49. The *dashed line* is a growing exponential which was fit to the data for $3 \le t \le 9$ s

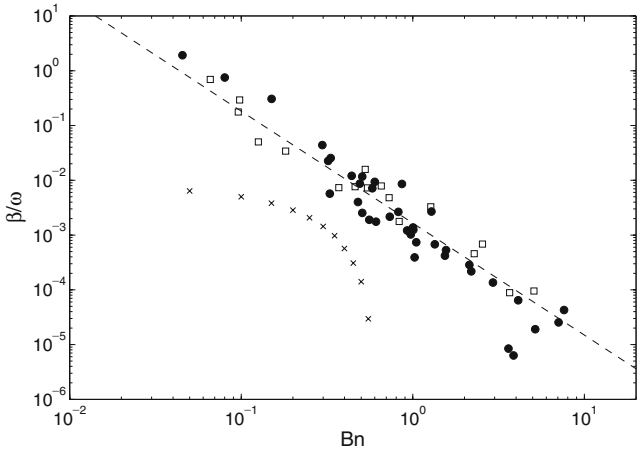

Fig. 9 The *circles* are the dimensionless exponential growth rates β/ω plotted as a function of Bingham number. *Open symbols* are for $c = 0.2\%$ and *solid symbols* for $c = 0.4\%$. The *crosses* are theoretical results for the dimensionless growth rate of the most unstable mode calculated for a yield-stress fluid flowing down an incline (Balmforth et al. 2007)

parameters, and the fit was performed over the range of times shown. This function describes the initial finger growth quite well in all runs for which fingers formed.

The Bingham number Bn is the dimensionless ratio of the force due to yield stress to viscous forces. Bn = 0 for a fluid with no yield stress and increases as the yield stress becomes relatively more important. In terms of the parameters of Eq. 1, Bn is given by

$$\mathrm{Bn} = \tau_0/K\dot{\gamma}^n, \tag{2}$$

where τ_0, K, and n are known from the rheological measurements presented above. We approximate the strain rate $\dot{\gamma}$ in our experiments by $\mathrm{d}r_{\max}/h\mathrm{d}t$, where $\mathrm{d}r_{\max}/\mathrm{d}t$, the radial velocity at the outermost point on the perimeter of the drop, is determined in the early stages of the run, before the radial strain exceeds the yield strain. We estimate the thickness of the drop h by taking it to be a cylinder with the same volume V and initial radius r_0, in which case $h = V/\pi r_0^2$. We find Bn to range from 0.04 to 100 in our experiments.

In Fig. 9, we plot the dimensionless exponential growth rate β/ω as a function of Bn for all of our runs. The data for $c = 0.2$ and $c = 0.4$ fall on a single curve and are well described by a power-law dependence of the form $\beta/\omega = (1.7 \pm 0.2) \times 10^{-3}\mathrm{Bn}^{-2.04\pm0.11}$.

Fingers form only for high enough values of the angular speed and initial radius r_0, as shown for $c = 0.4\%$ in Fig. 10a. The open circles indicate values of these parameters for which at least one finger was observed, while the filled circles indicate conditions for which the fluid drop remained approximately circular.

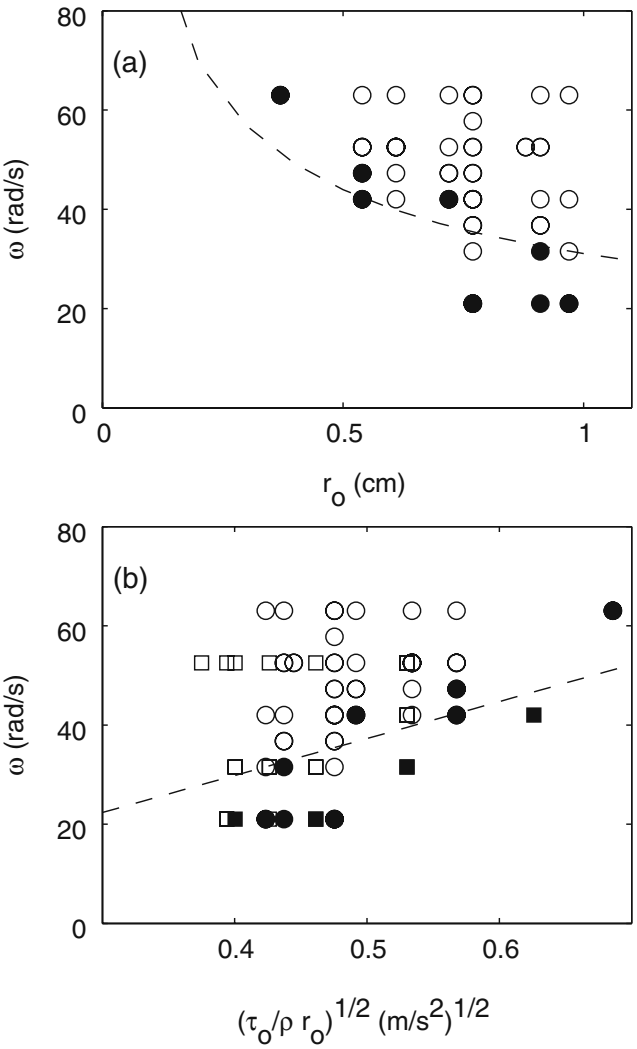

Fig. 10 **a** Experimentally determined stability boundary for $c = 0.4\%$. The *open symbols* correspond to parameters for which a finger(s) was seen while the *solid symbols* correspond to parameters for which fingering did not occur. The *dashed line* is the stability boundary predicted by Eq. 3 with $h_0 = 0.18$ mm. **b** ω vs $\sqrt{\tau_0/\rho r_0}$ for $c = 0.2\%$ (*squares*) and 0.4% (*circles*). *Open* and *solid symbols* have the same meaning as in **a**, and the *dashed line* again shows the prediction of Eq. 3 with $h_0 = 0.18$ mm

For $c = 0.2\%$, a similar boundary was obtained at lower values of ω and V.

Discussion

There are two possible mechanisms that could lead to the formation of the fingers we observe in our experiments. The first is the usual contact line instability that has been studied in Newtonian fluids, but modified by the presence of a yield stress (Balmforth et al. 2007). It is also possible that the fingers form as a result of

localized yielding of the material when the shear stress exceeds the yield stress at a particular point on the perimeter of the droplet.

In spin coating experiments using much larger volumes of yield-stress fluid, Tabuteau et al. (2007a) observed an instability in which many equally spaced fingers formed simultaneously. These fingers formed at an angular velocity well above that at which the stress due to the centrifugal force overcomes the yield stress (see Eq. 3 below), so the material in these experiments was essentially a shear-thinning liquid. Similarly, experiments on a sheet of yield-stress fluid flowing down an incline also showed a spatially periodic fingering instability (de Bruyn et al. 2002). The latter case has recently been treated theoretically (Balmforth et al. 2007). It seems probable that what was observed in these previous experiments was in fact the same contact line instability as that seen in Newtonian fluids (Melo et al. 1989; Fraysse and Homsy 1994; Holloway et al. 2007). As with other pattern-forming instabilities, this instability appears with a characteristic wavelength and grows uniformly everywhere along the entire contact line. At small amplitudes, the instability has a sinusoidal spatial dependence. Initially, the length of the fingers grows exponentially, then saturates as nonlinear effects become important (Fraysse and Homsy 1994; Holloway et al. 2007). Balmforth et al. (2007) found that the straight contact line of a flowing yield-stress fluid is unstable to perturbations over a range of wavenumbers for sufficiently small Bn. They showed that the exponential growth rate of disturbances with the fastest growing wavenumber decreased as the Bingham number increased, passing smoothly through zero and becoming negative at a particular value of Bn. The growth rates calculated by Balmforth et al. (2007) for a particular choice of material parameters are plotted as crosses in Fig. 9 for comparison with our experimental results.

The second possible mechanism—localized yielding—can be understood as follows. Consider a small droplet of yield-stress fluid in our experimental apparatus and imagine slowly increasing the angular velocity from rest. The shear stress σ in the material where it contacts the substrate is approximately given by $\sigma = \rho\omega^2 rh$, where ρ is the density, r the radial coordinate, and h is the thickness of the material (Tabuteau et al. 2007a), so it is largest at the contact line. If, as is unavoidably the case experimentally, the contact line is not perfectly circular, but rather has a small outward perturbation somewhere, then the shear stress will be highest at that perturbation. At sufficiently low angular velocities, the shear stress is less than the yield stress, so the material is everywhere unyielded and solid-like. At some value of the angular velocity, however, the shear stress at the outward perturbation will reach the yield stress, while remaining less than the yield stress elsewhere. At this point, the material in our perturbation will yield and the centrifugal force will cause it to flow outwards, forming a finger.

There are two significant differences between these two mechanisms. In the former, the yield stress is exceeded everywhere along the contact line and the material is essentially behaving as a shear-thinning liquid. Fingering in this case is the result of a pattern-forming instability, which affects the entire contact line. In contrast, in the latter case, the material is mostly solid and the yield stress is exceeded only locally, and finger formation is a purely local phenomenon that will have no effect on the contact line far away.

In our experiments, we do not see a sinusoidal disturbance with a characteristic wavelength, which grows uniformly around the contact line, but rather a single finger that develops locally (with the possibility of additional fingers developing independently later). More quantitatively, the growth rates of the fingers in our experiments decrease with an inverse power-law dependence on Bn, while those predicted for the traditional contact line instability go through zero and become negative at some value of the Bingham number as shown in Fig. 9.

We can also estimate the wavelength of the instability predicted for the yield-stress-modified contact line instability. The calculations of Balmforth et al. (2007) for the flow of a fluid layer down an inclined plane predict a maximum value of the wave number $k \approx 0.3$, in units of the inverse of a length scale L in the plane of the layer. For small droplets, the corresponding length scale must be of order r_0, the initial radius of the droplet. This gives a dimensional wave number of $0.3/r_0$, corresponding to a wavelength of order three times the circumference of the drop. This is clearly impossible, and implies that small droplets are stable against this instability. The situation changes for larger volumes of fluid—such as those used by Tabuteau et al. (2007a)—in which case the in-plane length scale becomes much smaller than the drop radius and the contact line instability can develop.

These results suggest strongly that the fingers observed in our experiments do not form as a result of an instability of the entire contact line, but instead form due to local yielding when the stress at a particular point on the perimeter of the drop becomes larger than the yield stress.

In the absence of contact line pinning, droplets of a fluid with no yield stress will spread for arbitrarily small ω when subjected to a centrifugal force. In our

case, however, the presence of a yield stress precludes any flow until the stress due to the centrifugal force exceeds τ_0, or equivalently, until the strain surpasses the yield strain γ_0. Following Tabuteau et al. (2007a), we estimate the force due to surface tension to be of the same order as that due to yield stress in our drops. In the absence of contact line pinning, surface tension will affect the shape of the fluid surface but will not of itself prevent motion of the contact line. If pinning does exist, flow cannot take place until the stress due to the centrifugal force exceeds the combination of the yield stress and the pinning force, but since the yield stress is a material property while the pinning force will vary depending on the microscopic conditions on the substrate, it is likely that the material will yield first at a point where the pinning force is small. Consequently, we do not expect surface tension or pinning to have a large effect on the observed behavior.

For strains smaller than γ_0, the unyielded Carbopol will respond elastically to the stress. The maximum radial strain reached by the Carbopol drops that did not finger does not exceed 0.066 for $c = 0.2\%$ and 0.17 for $c = 0.4\%$. These are consistent with measured values of γ_0 of approximately 0.2 for other yield-stress fluids (Coussot et al. 2006; Tabuteau et al. 2007b). The yield strain of our Carbopol samples can also be estimated from the rheological data presented in Figs. 1 and 2. Assuming the Carbopol is in the linear viscoelastic regime before it yields, γ_0 is related to the yield stress by $\tau_0 = G'(0)\gamma_0$ (Coussot et al. 2006), where $G'(0)$ is the zero-frequency elastic modulus. Using our rheological measurements, this gives $\gamma_0 = 0.02$ for $c = 0.2\%$ and $\gamma_0 = 0.024$ for $c = 0.4\%$, somewhat lower than the maximum strains observed for the non-fingering drops. The difference may be due to aging of the Carbopol during the time it sits on the plate before spinning, although aging is not expected to be important for Carbopol. More likely, it may indicate that evaporation from the surface of the small droplets affects the material properties, and in particular causes the yield stress τ_0 to increase over the time scale of the experiments.

Tabuteau et al. (2007a) considered a cylindrical volume of yield-stress fluid with radius r_0 and height $h_0 \ll r_0$ on a rotating substrate. They found the critical angular velocity ω_c at which the yield stress is exceeded to be

$$\omega_c = \sqrt{\frac{\tau_0}{\rho h_0 r_0}}. \tag{3}$$

Since our drops are not cylindrical, we do not expect Eq. 3 to be quantitatively accurate in our case, but we can nonetheless compare this prediction with our results. We take τ_0 from our rheological measurements and r_0 directly from our experimental images. h_0 is harder to measure accurately, so we treat it as an adjustable parameter in using Eq. 3 to describe the stability boundary seen in Fig. 10a. The result for $h_0 = 0.18$ mm is shown as a dashed line in Fig. 10a and gives good agreement with our experimental stability boundary. This value of h_0 is a reasonable estimate of the height of our drops and less than the calculated height at which gravitational force alone can overcome the yield stress (Tabuteau et al. 2007a). This supports our suggestion that a finger forms only when the centrifugal force causes the stress at some point around the perimeter of the drop to become greater than the yield stress.

Figure 10b shows the stability diagram for both $c = 0.2\%$ (squares) and 0.4% (circles) plotted as ω vs $\sqrt{\tau_0/\rho r_0}$. When plotted in this manner, the stability boundaries for the two concentrations coincide. The dashed line is the prediction of Eq. 3 with $h_0 = 0.18$ mm, which again shows reasonable agreement with the experimentally observed stability boundary.

For drops that finger, a well-developed ridge forms around the drop's perimeter as it spreads. Although in previous experiments, fingering resulted from an instability of a similar ridge (Melo et al. 1989; Fraysse and Homsy 1994; Holloway et al. 2007; Tabuteau et al. 2007a), in the present case, the formation of fingers appears to be a local phenomenon. Examination of images such as those in Figs. 3 and 4 suggests that the formation of a finger affects the ridge in the immediate vicinity of the finger, but not elsewhere. This in turn implies that the presence of a finger does not relax the stress field far away so that additional, independent fingers can form elsewhere when the stress becomes large enough there.

Finally, we note that, although the experiments of Tabuteau et al. (2007a) were carried out using a material with a yield stress a factor of 50 larger than ours, and with samples a factor of 100 larger in volume, our results are consistent with the initial stages of those of Tabuteau et al. (2007a). At low rotation rates, below the critical value of ω at which the solid–liquid transition occurs, they observe a regime in which the height of their initially cylindrical sample decreases while its radius increases. In this regime, they observe the radial strain to saturate after some time, with a maximum strain of about 12%. This is very similar to the behavior we see in the case of drops that do not finger. Above the critical rotation rate, their drops continue to spread, and at high rotation rates, a roll forms at the perimeter of their sample. At the largest values of ω, they observe a modulation of the roll that leads to the formation of fingers. With the exception of the mechanism of finger

formation, this behavior is again qualitatively similar to that observed in the present work. Thus, despite the somewhat different material properties and experimental conditions, the only qualitative difference between the results of Tabuteau et al. (2007a) and our results is that they see a fingering instability that appears with a characteristic wavelength in the late stage of the flow, while we see the formation of a single finger relatively early in the flow. This difference is due to the fact that our experiments involve very small droplets, and the centrifugal force in our experiments is comparable to the force due to the yield stress. At low angular velocities, our materials remain unyielded, and our fingers form coincident with the transition from solid to fluid behavior. In contrast, the materials in the above work were well above the flow threshold when the fingering occurred. Under our experimental conditions, the fingering occurs by local yielding of an otherwise largely solid-like material, and the usual contact line instability is preempted.

Conclusion

We have studied spreading and fingering during spin coating of small droplets of a material with a weak yield stress. In contrast to what has been observed in the absence of a yield stress, fingers do not form collectively as the result of an instability of the contact line, but rather form individually when the stress due to the centrifugal force exceeds the yield stress locally. When the stress at the perimeter of the drop due to the centrifugal force is small, drops of the fluid deform elastically by a small amount, then stop. For high enough drop volumes and rotation speeds, the spreading continues until the stress at some point on the perimeter exceeds the yield stress, at which point a single finger starts to form at that point. The rate at which spreading occurred for drops that finger increases with increasing V and increasing ω.

Acknowledgement This research has been supported by the National Sciences and Engineering Research of Canada.

References

Acrivos A, Shah MJ, Petersen EE (1960) On the flow of a non-Newtonian liquid on a rotating disk. J Appl Phys 31:963–968
Balmforth N, Ghadge S, Myers T (2007) Surface tension driven fingering of a viscoplastic film. J Non-Newton Fluid Mech 142:143–149
Borkar AV, Tsamopoulos JA, Gupta SA, Gupta RK (1994) Spin coating of viscoelastic and nonvolatile fluids over a planar disk. Phys Fluids 6:3539–3553
Burgess SL, Wilson SDR (1996) Spin-coating of a viscoplastic material. Phys Fluids 8:2291–2297
Carnali JO, Naser MS (1992) The use of dilute solution viscometry to characterize the network properties of carbopol microgels. Colloid Polym Sci 270:183–193
Coussot P, Tabuteau H, Chateau X, Tocquer L, Ovarlez G (2006) Aging and solid or liquid behavior in pastes. J Rheol 50: 975–994
de Bruyn JR (1992) Growth of fingers at a driven three-phase contact line. Phys Rev A 46:R4500–R4503
de Bruyn JR, Habdas P, Kim S (2002) Fingering instability of a sheet of yield-stress fluid. Phys Rev E 66:031504-1-5
Emslie AG, Bonner FT, Peck LG (1957) Flow of a viscous liquid on a rotating disk. J Appl Phys 29:858–862
Fraysse N, Homsy GM (1994) An experimental study of rivulet instabilities in centrifugal spin coating of viscous Newtonian and non-Newtonian fluids. Phys Fluids 6:1491–1504
Holloway KE, Habdas P, Semsarillar N, Burfitt K, de Bruyn JR (2007) Spreading and fingering in spin coating. Phys Rev E 75:046308-1-5
Jenekhe SA, Schuldt SB (1985) Flow and film thickness of Bingham plastic liquids on a rotating disk. Chem Eng Commun 33:135–147
Jerrett JM, de Bruyn JR (1992) Fingering instability of a gravitationally driven contact line. Phys Fluids A 4:234–242
Lemaire E, Levitz P, Daccord G, Van Damme H (1991) From viscous fingering to viscoelastic fracturing in colloidal fluids. Phys Rev Lett 67:2009–2012
Lindner A, Coussot P, Bonn D (2000) Viscous fingering in a yield stress fluid. Phys Rev Lett 85:314–317
McKinley IS, Wilson SK, Duffy BR (1999) Spin coating and air-jet blowing of thin viscous drops. Phys Fluids 11:30–47
McKinley IS, Wilson SK (2002) The linear stability of a drop of fluid during spin coating or subject to a jet of air. Phys Fluids 14:133–142
Melo F, Joanny JF, Fauve S (1989) Fingering instability of spinning drops. Phys Rev Lett 63:1958–1961
Noveon (2002) Noveon Technical Data Sheet #216. http://www.pharma.noveon.com/literature/tds/tds216.pdf
Schwartz LW (1989) Viscous flows down an inclined plane: instability and finger formation. Phys Fluids A 1:443–445
Spaid MA, Homsy GM (1994) Viscoelastic free surface flows: spin coating and dynamic contact lines. J Non-Newton Fluid Mech 55:249–281
Spaid MA, Homsy GM (1996) Stability of Newtonian and viscoelastic dynamic contact lines. Phys Fluids 8:460–478
Spaid MA, Homsy GM (1997) Stability of viscoelastic dynamic contact lines: an experimental study. Phys Fluids 9:823–832
Tabuteau H, Baudez JC, Chateau X, Coussot P (2007a) Flow of a yield stress fluid over a rotating substrate. Rheol Acta 46:341–355
Tabuteau H, Oppong F, de Bruyn JR, Coussot P (2007b) Drag on a sphere moving through an aging system. Europhys Lett 78:68007-1-5
Togashi S, Ohta T, Azuma H (2001) Fingering flow pattern of a liquid film on a rotating substrate. J Chem Eng Jpn 34:1402–1406
Troian SM, Herbolzheimer E, Safran SA, Joanny JF (1989a) Fingering instabilities of driven spreading films. Europhys Lett 10:25–30
Troian SM, Wu XL, Safran SA (1989b) Fingering instability in thin wetting films. Phys Rev Lett 62:1496–1499
Tsamopoulos JA, Chen MF, Borkar AV (1996) On the spin coating of viscoplastic fluids. Rheol Acta 35:597–615
Wang M-W, Chou F-C (2001) Fingering instability and maximum radius at high rotational Bond number. J Electrochem Soc 148:G283–G290